CORROSION AND CAVITATION IN TUBE FURNACES DURING THE HEATING OF WATER - CONTAMINATED OIL

Serhiy Nesterenko[1], Denis Miroshnichenko[2, 3], Leonid Bannikov[3], Olexandr Borisenko[3], Volodymyr Tertychnyi[2], Maxim Bichev[1]

[1]*O. M. Beketov National University of Urban Economy*
17 Marshal Bazhanov St., Kharkiv, Ukraine, 61002, nesterhnamg@gmail.com (S.N.).
[2]*National Technical University Kharkiv Polytechnic Institute*
2 Kyrpychova St., 61002 Kharkiv, Ukraine, dvmir79@gmail.com (D.M.);
volodymyr.tertychnyi@ihti.khpi.edu.ua (V.T.).
[3]*Ukrainian State Research Institute for Carbochemistry*
7 Vesnina St., Kharkiv, Ukraine, 61023, ukhinbannikov@gmail.com (L.B.);
zd@ukhin.org.ua (O.B.).

Received 09 December 2025
Accepted 27 January 2026 *DOI: 10.59957/jctm.v61.i4.2026.10*

ABSTRACT

In coking plants, tube furnaces are used to heat tar and oils, playing a crucial role in steam conservation. As a relatively expensive installation, they require careful maintenance to ensure serviceability and safe operation. Heating water-contaminated oil in a tubular furnace leads to severe metal corrosion, characterized by hemispherical cavities. The study of metal structure was carried out by light microscopy (metallographic method) on specially made micro disks. While intergranular corrosion is absent, signs of cavitation-induced damage are evident. Water contamination significantly increases the vapor phase fraction, particularly at reduced flow pressure and elevated temperatures, promoting cavitation and erosion within the tube bundle. Hydraulic calculations indicate that under turbulent flow conditions, with a pressure of 1 bar, 20 % water content, and a temperature of 160°C, cavitation becomes inevitable. This phenomenon accelerates corrosion, especially in the presence of aggressive compounds such as ammonium chloride. Electrochemical analysis confirms a high corrosion rate in oil contaminated with water.

Gravimetric measurements reveal the aggressive nature of oil vapours toward carbon steel due to the release of corrosive coke oven gas components (H_2S, NH_3, HCN). The findings highlight the critical role of cavitation in corrosion processes and emphasize the need for controlling water contamination in oil heating systems to mitigate equipment degradation.

Keywords: tube furnace, coal tar oil, corrosion, metallographic method, cavitation.

INTRODUCTION

At existing coke plants, the modernization of outdated equipment is accompanied by the introduction of compact, metal - efficient units. This approach necessitates the use of new materials that have not previously been employed in aggressive and complex technological environments. Consequently, selecting corrosion - resistant materials has become a critical task for various units in the chemical sector of coke production, including those for benzene recovery and processing [1, 2], hydrogen sulfide removal [3, 4], coal tar processing [5], and coke oven gas transportation [6].

One of the most expensive components of chemical plant equipment is the heat transfer surfaces of tubular furnaces, which are used for the distillation of coal wash oil and the heating of tar before rectification [7]. The similarity in the composition of the processed media allows for a comparative analysis of the failure mechanisms of tube bundles operating under conditions of heating by coke gas combustion products.

Identifying the causes of inner surface corrosion in tubular furnace tubes within the coke - chemical and oil refining industries is a critical task, as corrosion can significantly reduce equipment reliability, shorten service life, and lead to emergency failures with substantial

economic losses. Studies indicate that the main factors contributing to corrosion include manufacturing and welding defects, residual stresses, improper material selection and design choices, the aggressiveness of the process environment, the presence of corrosive components (Cl^-, S_x^-, NH_4^+), as well as deviations from regulated operating conditions and non - compliance with standard shutdown procedures [8].

In order to reduce risks in design, special attention is paid to the parameters of furnace operation, which have a significant impact on operational safety, the rate of coke accumulation in the pipes and the duration of the overhaul period [9].

A frequent cause of failure of oil heating pipes is destruction of their inner surface caused by corrosion under deposits. Solid deposits in pipelines create localised environments chemically and physically different from clean areas, which lead to accelerated corrosion under the deposits, formation of cracks and pitting [10]. Coke accumulation also leads to overheating of heat transfer surfaces.

Premature failure of tube furnaces is often caused by impurities in crude oil, particularly trace amounts of metals and chlorides [11]. High - temperature corrosion from chloride - containing impurities leads to the degradation of furnace tubes, necessitating the use of high - grade alloys resistant to such aggressive environments [12]. To reduce the chloride content in tar entering the tube furnace, coke - chemical plants employ soda treatment. This method effectively removes chloride - containing compounds from the tar, helping to mitigate corrosion and extend equipment service life [5].

Sulfide corrosion is a common failure mechanism in tar and oil refineries. It occurs due to the chemical interaction between sulfur - containing compounds in the raw materials and the pipe material, leading to wall thinning and a reduction in equipment strength [13].

The sulfur content in crude oil ranges from 0.89 to 5.67 wt. % [14]. The main sulfur - containing compounds in petroleum products include thiols, sulfides, thiophenes, sulfoxides, and sulfones [15]. In coal tar, the sulfur content can reach up to 4% [16]. In coal absorption oil, sulfur content typically ranges from 0.3 % to 0.6 %, but it can increase to 5.3 % in waste oil during operation [17]. Additionally, an increasing number of previously unidentified sulfur - containing compounds, such as thioxanthene isomers, have been detected in coal tar [18].

A distinctive feature of sulfide corrosion during the refining of sulphur - rich oil in the temperature range of 230 - 425°C is the simultaneous presence of sulphur - containing compounds and naphthenic acids. To enhance material resistance to sulfide corrosion, the chromium content in steel is increased [19].

A key aspect of heating materials in tube furnaces is maintaining an appropriate velocity of the heated fluid to prevent coking and ensure high heat transfer efficiency. However, it is known that when flue gas - heated water flows at a pressure of 10 bar and a temperature of 160°C through elbow tubes made of mild steel, cavitation and erosion processes occur [20]. These processes begin with the formation of a rough, jagged surface, and the smaller the radius of the elbow, the greater the severity of cavitation erosion.

As pressure drops in the evaporator, where heated water enters the elbow tube, turbulence increases due to partial vaporization of the working fluid, forming a two - phase flow of water and vapor. This further intensifies cavitation - erosion effects [20]. Similar processes can contribute to tube corrosion in a furnace when heating coal wash oil, where water present as an emulsion can trigger cavitation effects, leading to accelerated surface degradation [20].

A review of existing studies highlights a significant gap in data regarding the factors contributing to tube bundle failures in tube furnaces during the pumping of coal tar and its fractions. Specifically, there is a lack of detailed information on how operating parameters - such as temperature, pressure, and flow rate - affect the durability of tube bundles when processing coal tar and its diverse fractions. Investigating the mechanisms of pipe corrosion and wear under the influence of coal tar components could lead to the development of more effective corrosion prevention strategies and extend equipment service life in the the coke chemical industry.

EXPERIMENTAL

The research was conducted in the benzene department, which had long operated a 3D 2 - 215/9 type tubular furnace equipped with a tube bundle made of 15Kh5M cracking steel. Frequent equipment malfunctions and the discontinuation of oil spraying in the benzene absorber allowed gas water condensate

to enter the under - scrubber collection tank. When the centrifugal pump was activated, the oil became emulsified with water, leading to the tube furnace operating for extended periods with oil containing 4 - 8 % water. The oil quality worsened due to inadequate cooling before reaching the absorber, promoting the evaporation of light fractions and increasing the oil's viscosity and tendency to adhere.

Due to the difficulty of representation, the aggressive effect of oil on equipment in laboratory conditions, the research methodology was based on the determination of the corrosion rate in industrial conditions according to ASTM International Standard [21]. After degreasing and weighing, coupons of various materials of 60×60 mm size were placed in hot oil pipelines (Table 1).

The corrosion rate values were determined from four parallel measurements conducted on manufactured samples of each steel type. After testing, the specimens were removed from the equipment, weight reduction was determined and the average corrosion rate was calculated from it. The corrosion rate values were determined from four parallel measurements conducted on manufactured samples of each steel type.

Aqueous extracts were prepared and analysed to assess the corrosion aggressiveness of oils [22]. A tenfold volume of distilled water was added to the oil sample and boiled for 0.5 h with a reflux condenser, after which the aqueous layer was filtered through a paper filter.

Laboratory electrochemical corrosion studies were conducted using a standard three-electrode cell with separated interelectrode spacings to construct polarization curves. A saturated calomel electrode (SCE) served as the reference electrode, and a platinum wire was used as the counter electrode with the counter electrode of 3.5 cm^2 surface area. The working electrode with a surface area of 3.1 mm^2 was fabricated from structural carbon steel (St. 3). Prior to each experiment, the St. 3 steel working electrode was polished to a 600 - grit finish using silicon carbide paper, then rinsed with deionized water and degreased with acetone. Measurements were performed using a voltammetric potentiostat (MTech COR - 50F) interfaced with a personal computer. The temperature of the solution was maintained at 50°C throughout the measurements using a U - 10 thermostat.

The corrosion current density, which is proportional to the corrosion rate of the metal in the investigated medium, was determined by Tafel extrapolation. Tafel slopes were determined by linear regression of the polarization curves in the potential range of ±150 mV vs. SCE. The corrosion rate (K) was calculated using the following Eq. (1):

$$K = \frac{i \times A}{n \times 2.68 \times 10^{-2}}, \text{ g m}^{-2} \text{ hr}^{-1} \quad (1)$$

where A is the atomic mass of iron, n is the number of electrons participating in the electrochemical reaction, and i is the corrosion current density, A cm^{-2}.

The study of the metal structure was conducted using light microscopy (metallographic method) on specially prepared micro disks.

Samples were prepared with bevelled corners on the surface of a microdrill, shaped as a square with side lengths of 10 - 20 mm and a height of 10 - 15 mm. The microdrill surface was levelled through coarse grinding, followed by fine grinding performed on an FTP-1M grinding and polishing machine. Subsequently, lapping

Table 1. Chemical composition of steels selected for testing.

Steel grade	Content of alloying components, %						
	C	S	P	Cr	Ni	Mo	Mn
AISI 501	0.17	0.020	0.035	4.8	-	0.45	-
AISI 430Ti	0.10	0.010	0.023	17.1	-	-	-
AISI 202	0.12	0.020	0.030	17.0	4.0	-	9.1
AISI 309Ti	0.18	0.010	0.030	23.5	13.0	-	0.27
AISI 304	0.08	0.030	0.045	19.0	9.3	-	-
AISI 316	0.08	0.030	0.045	18.7	12.0	2.4	-
AISI 410	0.08	0.030	0.040	11.5	0.6	-	-
AISI 1020	0.22	0.035	0.035	-	-	-	≤ 0.55

was conducted on a grinding wheel coated with abrasive particles in the form of pastes. Polishing was then performed on a polishing machine with a felt - covered disc. The resulting sample (slip) was etched using a 5 % HNO_3 solution in ethyl alcohol. The etched slip was examined under a microscope at a low magnification of 100×. For the microstructural analysis of the materials, an Optika IM - 3MET metallographic inverted microscope was used to observe the microslides [23].

Oil impurities were identified using a Neophot microscope in reflected light, digital photographs of the samples were obtained and processed using a ToupTech instrument with ToupView software.

The identification and measurement of element concentrations were performed using an ElvaX ProSpector 2 X - ray fluorescence spectrometer (Elvatech LLC, Ukraine). The device analyses elements ranging from Mg to U utilizing an X - ray tube with a W - anode (maximum voltage: 40 kV, maximum current: 100 μA) and a thermoelectrically cooled PIN - diode detector (active area: 6 mm^2, energy resolution: < 180 eV at 5.9 keV).

RESULTS AND DISCUSSION

The tube furnace of the benzene department was frequently stopped for repairs to replace sections of the tube bundle with a diameter of 127×10 mm and a length of 10 m. The nature of the damage is shown in Fig. 1.

The inner surface of the pipe is covered with oxide deposits exhibiting an uneven, rough structure with spots of varying intensity. The surface also features localized depressions, including through - penetrating ones, as well as notches, cracks, and irregularities in the metal, likely resulting from localized mechanical effects.

From a fragment of the pipe (Fig. 1) that had undergone severe corrosion damage, Sample 1 and Sample 2 were extracted and prepared for microstructure examination. Visual inspection of the provided sample segment revealed a defect originating at the metal surface and extending deep into the sample. This defect fully penetrates the sample, emerging on the opposite side, and resembles an irregular crater. Such a defect is identified as pitting corrosion, the most destructive form of localized attack, characterized by the formation of holes in the metal. This type of corrosion is typical of stainless steels in chloride - containing environments.

Micrographs of the specimens and fracture assessment are shown in Fig. 2 and Table 2 respectively, the results of XRF analysis of the specimens are shown in Table 3.

The microstructural analysis of 15Kh5M cracking steel samples revealed a heterogeneous distribution of non-metallic inclusions. According to Table 2, both samples exhibit a high content of point oxides and undeformed silicates, with point oxide scores ranging from 4.0 - 5.0. The scoring system (Table 2) is based on ISO 4967:2013, where the number of points corresponds to the relative amount and size of non-metallic inclusions (oxides and silicates) observed in the

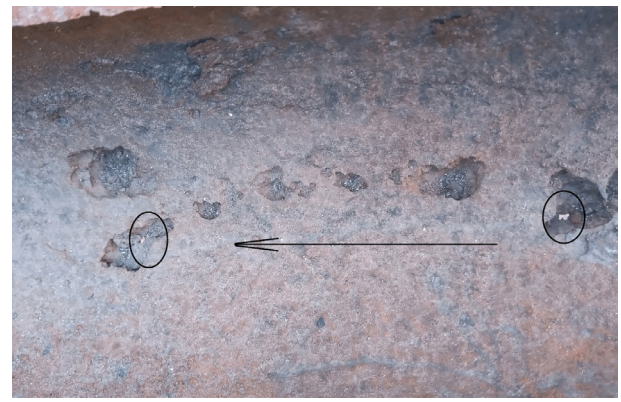

Fig. 1. Cross-section of the damaged pipe: the arrow indicates the direction of oil flow, and the through-holes are enclosed by an ellipse.

Table 2. Comparative assessment of oxide and silicate inclusions in 15Kh5M steel samples.

Parameter	Sample 1	Sample 2
Point oxides, points	4.0 - 4.5	4.5 - 5.0 with zones scoring 2.0
Layered silicates, points	2.0	2.0
Undeformed silicates, points	4.0 - 4.5 with zones scoring 3.5	4.0 - 5.0 with zones scoring 3.0
Brittle silicates, points	4.0 with zones scoring 2.0	4.0 with zones scoring 2.0

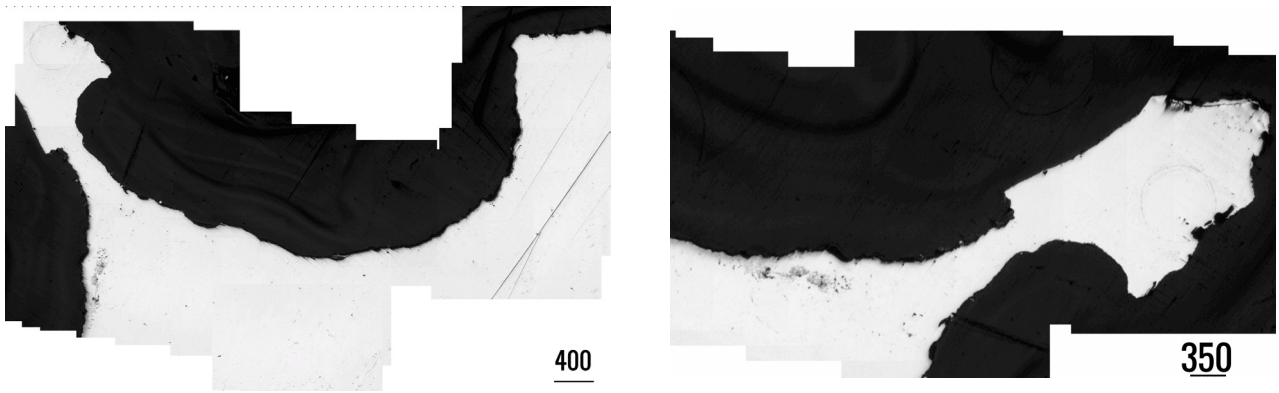

Fig. 2. Corrosion fracture areas of sample 1 (a) and sample 2 (b). Numbers in the images denote the size, μm.

Table 3. Metal composition of provided 15Kh5M steel samples, wt%.

Elements	Sample 1	Sample 2
	pipe elbow δ = 7 mm	pipe elbow δ = 8 mm
C	0.10	0.10
Si	0.40	0.36
Mn	0.43	0.38
P	0.013	0.013
S	0.07	0.04
Cr	4.69	4.15
Ni	0.17	0.25
Cu	0.19	0.19
Mo	0.40	0.45

microstructure. Higher scores indicate greater inclusion content. Notably, Sample 2 presents localized zones with reduced severity (scoring 2.0), suggesting some regional inhomogeneity in oxide distribution. Layered silicates are present at a consistent, moderate level (2.0 points) in both samples, indicating uniform occurrence of these inclusions. The undeformed silicates show slightly higher variability, with Sample 2 reaching up to 5.0 points, accompanied by zones of lower severity (3.0), possibly reflecting localized inclusion clusters. Brittle silicates exhibit identical scores across both samples (4.0 overall, 2.0 in specific zones), suggesting a comparable risk of crack initiation due to these inclusions. The distribution and morphology of these non-metallic inclusions could significantly influence the fracture resistance and operational performance of the steel, particularly in high-temperature cracking environments.

The chemical composition of the two 15Kh5M steel samples shows overall conformity with the typical specification range for this alloy, with minor variations between the samples. Both samples exhibit identical carbon (0.10 %) and phosphorus (0.013 %) content, ensuring comparable baseline hardenability and grain boundary behaviour. Sample 1 contains slightly higher levels of silicon (0.40 % vs. 0.36 %) and manganese (0.43 % vs. 0.38 %), which may provide marginally increased deoxidation and strengthening effects. Notably, chromium content is higher in Sample 1 (4.69 %) than in Sample 2 (4.15 %), potentially enhancing its corrosion and oxidation resistance. In contrast, Sample 2 contains slightly more nickel (0.25 % vs. 0.17 %) and molybdenum (0.45 % vs. 0.40 %), which may contribute to improved toughness and creep resistance. Sulfur content is higher in Sample 1 (0.07 %) compared to Sample 2 (0.04 %), which could negatively impact hot workability and promote inclusion formation. These

compositional differences, though within acceptable limits, may influence the corrosion behaviour of the steel in service.

Corrosion damage exhibits a hemispherical shape, with no evidence of intergranular corrosion (Fig. 3). Additionally, signs of cavitation-induced metal degradation were observed.

When the oil flow moves and heats up, a vapor phase containing benzene hydrocarbons forms, which is a normal condition for the distillation of wash oil. An increase in the vapor phase fraction is observed during process disturbances and oil watering. The calculation of vapor phase fraction values is based on the chromatographic composition of the absorbing oil across the range of its operating heating temperatures (Figs. 4 and 5).

As indicated by the above data, oil watering results in a substantial increase in the vapor phase fraction, often by an order of magnitude or more. Reduced pump pressure and elevated heating temperatures further increase the vapor fraction of the oil. The formation and collapse of vapor bubbles can lead to erosion and mechanical damage on the heat exchanger surface. Cavitation occurs when a sudden pressure drop in the fluid causes the formation and subsequent collapse of vapor bubbles, resulting in significant damage to the heat exchanger surfaces. The cavitation number (CN) is defined as the ratio of the difference between the absolute pressure and the saturated vapor pressure to the velocity head of the flow (Eq. (2)) [24]:

$$CN = \frac{P - P_s}{{}^1/_2 \rho V^2} \quad (2)$$

where: P - absolute pressure, Ps - saturated vapor pressure, ρ - liquid density, V - characteristic flow velocity. Calculations of the hydraulic parameters of the oil flow indicate that the motion is turbulent. The risk of cavitation (K ≈ 1) arises only when the pressure drops to P = 1 bar. As the pressure generated by the pump increases, the cavitation number rises by a factor of 4 - 12. The greatest risk of cavitation occurs at a pressure of 1 bar with watered oil (20 % water content) and a heating temperature of 160°C (K = 0.86); under these conditions, cavitation becomes inevitable.

The relative changes in the criteria as a function of temperature, for the reference point $Re_o = 1.44 \times 10^6$ and $K_o = 4.1$ (at t = 160°C, P = 4.0 bar, and 20 % water in oil), are presented in Fig. 6.

Fig. 3. Corrosion damage observed on the etched slip. The numbers in the images indicate the sizes, μm.

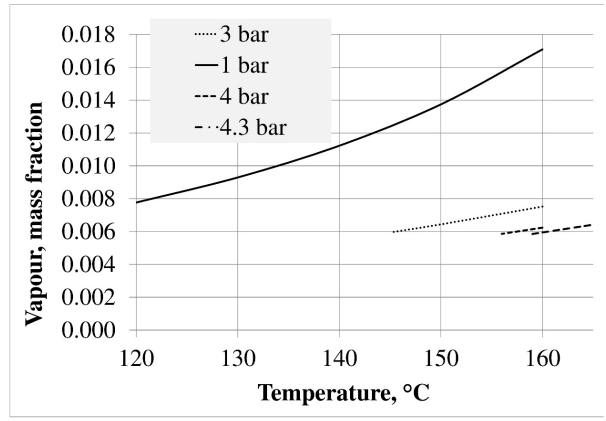

Fig. 4. Estimated values of the mass fraction of vapours during heating of oil with water content of 0.5 wt. %.

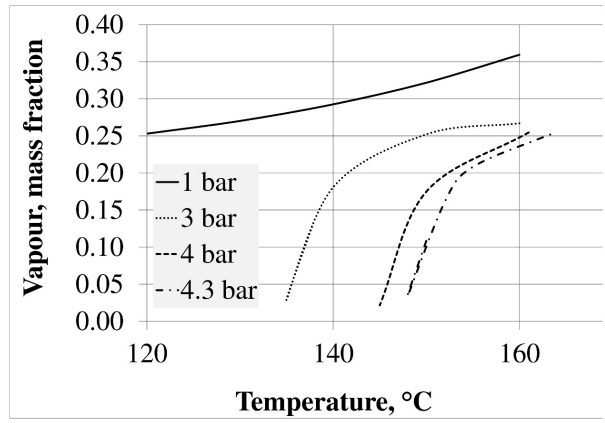

Fig. 5. Estimated values of the mass fraction of vapours during heating of oil with water content of 50 wt. %.

The calculations indicate that for oil without water, the physicochemical properties of the oil result in the Reynolds number and cavitation number remaining constant (Fig. 6, cvs. 1, 2). In contrast, the physicochemical properties of highly watered oil cause these parameters to become temperature-dependent (Fig. 6, cvs. 3, 4): flow turbulence increases as temperature decreases, while the risk of cavitation increases as temperature rises. It should be noted that in the presence of damage (such as potholes in pipes), a pressure drop in certain zones may occur, potentially leading to localized boiling of the oil.

The water content in the working absorption oil of the benzene compartment must not exceed 0.5 %. Oil watering may occur if the oil supply to the absorber is halted while gas continues to pass through it. In the case under consideration, the water content increased to 8 % and, in rare emergency situations, could reach 50 %. Fig. 7 presents microphotographs of the corresponding emulsions.

From micrographs of the emulsions, we measured the diameters of approximately 500 droplets and calculated the number - average droplet diameter (D_N) using the Eq. (3):

$$D_N = \Sigma (N \times d) / \Sigma N \quad (3)$$

where N is the number of droplets with diameter d included in the analysis.

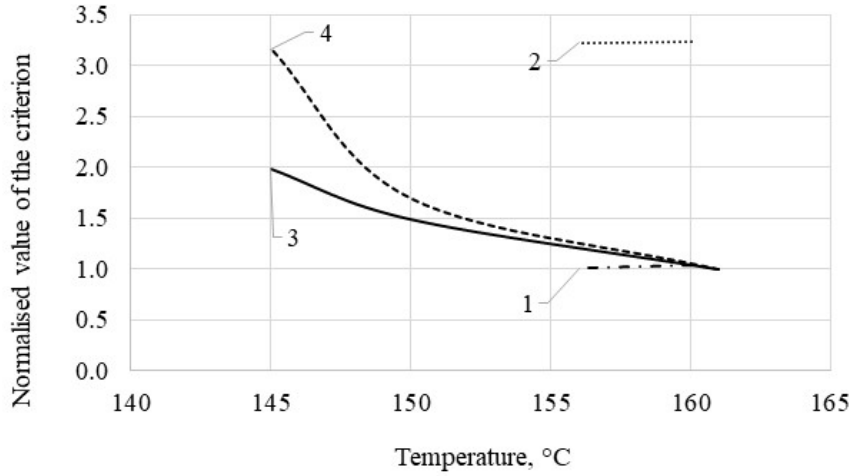

Fig. 6. Relative change in Reynolds number (Re/Re_0) and cavitation number (K/K_0). 1 - Re/Re_0 (0.5 % water in oil); 2 - K/K_0 (0.5 % water in oil); 3 - Re/Re_0 (20 % water in oil); 4- K/K_0 (20 % water in oil).

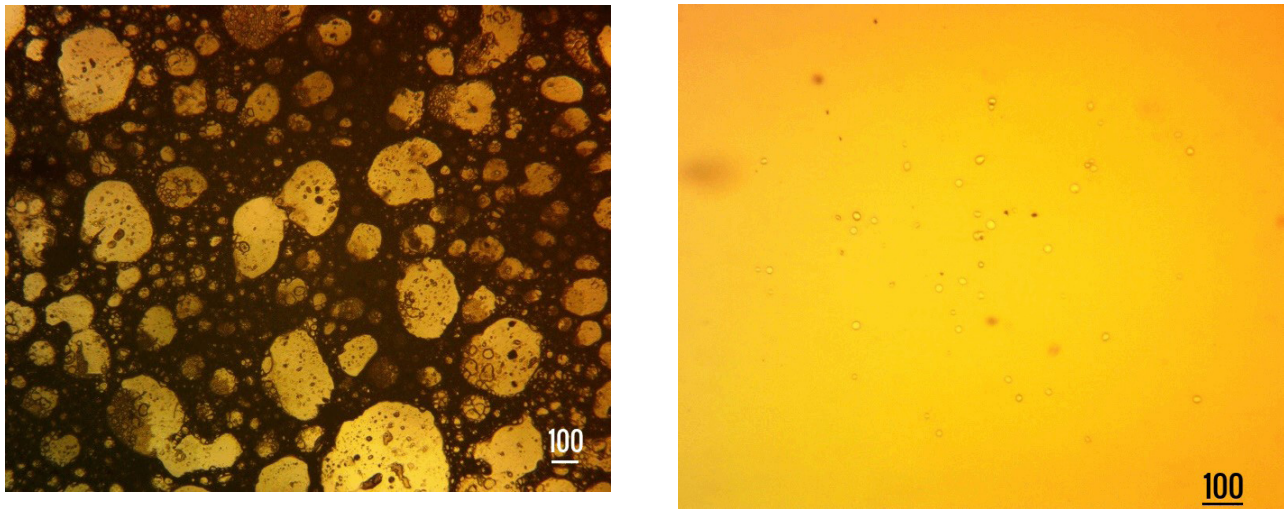

Fig. 7. Photomicrographic images of samples for two different water contaminations of oil: (a) 50% water and 8% water at ×100 magnification.

The polydispersity index (P_D) is defined as (Eq. (4)):

$$P_D = D_v / D_n \quad (4)$$

where D_v is calculated according to Eq. (5):

$$D_v = \Sigma (N \times d^4) / \Sigma (N \times d^3) \quad (5)$$

The measure of dispersibility is the specific interfacial surface (S_d), which is the ratio of the total surface area of the droplets to their total volume (Eq. (6)):

$$S_d = (\pi D_N^2)/(\pi D_N^3/6) = 6/D_N \quad (6)$$

Droplet-size characteristics and distribution indexes were determined in accordance with ISO 9276-2, which defines calculation procedures for number- and volume-weighted diameters and derived dispersity indices. Characteristics of disperse composition of emulsions are presented in Table 4.

An emulsion with a water content of 8 % is classified as a medium - disperse system. It exhibits a relatively homogeneous composition with a narrow range of droplet sizes, indicating low polydispersity. With a polydispersity index (P_D) value of less than 2, such emulsions are considered structured.

An emulsion with a water content of 50 % is classified as a low - disperse (coarse - disperse) system. It is characterized by a wide range of droplet sizes, indicating high polydispersity and compositional heterogeneity.

Low water content (8 %), small droplet size (maximum 29 μm), low polydispersity (P_D = 1.3), and high specific interfacial surface area (0.37 μm^{-1}) make it less prone to cavitation. The fine droplets and uniform water distribution reduce the likelihood of abrupt evaporation and vapor bubble formation [25].

In contrast, high water content (50 %), the presence of large droplets (up to 229 μm), high polydispersity (PD = 4.8), and low specific interfacial surface area (0.16 μm^{-1}) significantly increase the propensity for cavitation. The substantial water content and large droplets promote rapid vapor formation during heating [26].

Cavitation can accelerate corrosion processes, particularly in the presence of aggressive chemical compounds such as ammonium chloride. Hydrogen chloride is released during the coking of coal and accumulates in the water during infrequent purging of the washing cycle in the final cooling stage of coke oven gas, reaching chloride concentrations of 4000 - 6000 $mg \times dm^{-3}$. Along with splashes of entrained washing water, these chlorides enter the wash oil, intensifying local corrosion, especially when the oil becomes watered.

The presence of chlorides and thiocyanates in the aqueous extract leads to an increase in the corrosion current density and, consequently, to a higher corrosion rate of carbon steel, as determined by the potentiodynamic method (Fig. 8, Table 5).

The curve reflects the electrochemical behaviour of carbon steel in the presence of dissolved corrosive species extracted from the oil.

The operating oil is therefore in an unsatisfactory condition, as evidenced by its increased acidity and the accumulation of dissolved salts, particularly chlorides, which significantly contribute to accelerated electrochemical corrosion.

The corrosiveness of the vapor phase of the heated oil was assessed by suspending witness samples in the benzene column medium and analysing them using the gravimetric method. To evaluate the resistance of structural materials in benzene compartment

Table 4. Dispersibility properties of water-in-oil emulsions.

Indicators	Water content in emulsion, vol. %	
	8	50
Minimum droplet diameter, μm	5	1
Average droplet diameter, D_N, μm	16	38
Maximum droplet diameter, μm	29	229
Polydispersity index, P_D	1.3	4.8
Specific interfacial surface, μm^{-1}, S_d	0.37	0.16

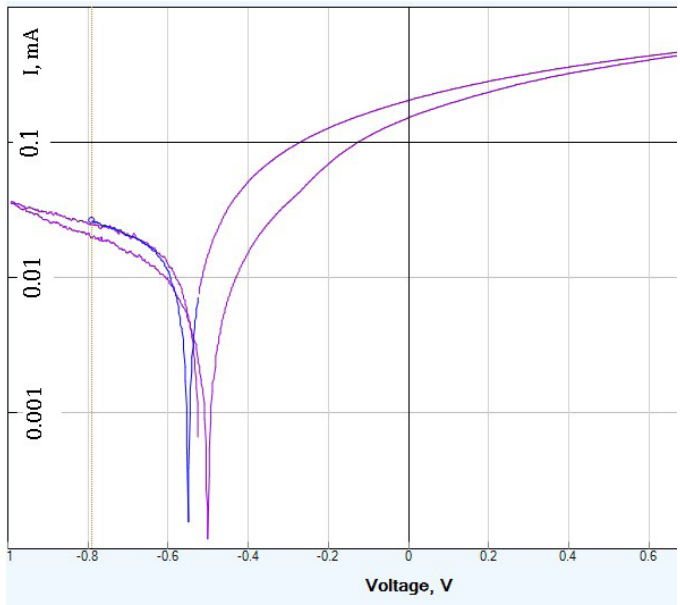

Fig. 8. Potentiodynamic polarization curve of the aqueous extract of the operating oil at 50°C, recorded at a potential sweep rate of 10 mV min^{-1}.

Table 5. Characterisation of the aqueous extract of the operating oil in comparison with units operating in normal mode.

Indicators	Operating wash oil from the benzene plant	
	Investigated	Normally operating
pH	4.92	6.7 - 7.2
Total salt content, mg L^{-1}	870	200 - 250
Chloride content, mg L^{-1}	260	100 - 120
Carbon steel corrosion rate, g m^{-2} h^{-1}, at 50°C	0.97	0.05 - 0.10

Table 6. Corrosion rate of carbon and alloy steels in benzene distillation column vapours, determined by the gravimetric method.

Steel grades		Corrosion rate, mm $year^{-1}$
Traditional term	Analogue	
St.3	AISI 1020 (carbon structural steel)	2.7690
08Kh13	AISI 410 (martensitic stainless steel)	0.1020
15Kh5M	AISI 501 Low-alloyed martensitic heat-resistant steel	0.3810
08Kh17T	AISI 430Ti (ferritic stainless steel alloyed with titanium)	0.0196
10Kh14G14N4T	AISI 201 (austenitic steel with high manganese content)	0.0388
12Kh17G9AN4	AISI 202 (austenitic stainless steel)	0.0256
08Kh22N6T	AISI 309Ti (heat resistant austenitic steel alloyed with titanium)	0,0097
08Kh18N10T	AISI 321 (austenitic stainless steel stabilised with titanium)	0.0059
10Kh17N13M2T	AISI 316Ti (austenitic corrosion resistant steel with Mo and Ti)	0.0011

environments, corrosion tests were conducted on samples of steels and selected alloys in the reboiler of the benzene compartment and in the vapor pipeline downstream of the distillation column. The test results are presented in Table 6.

Thinning of alloyed steel samples occurs uniformly, whereas in carbon steel samples, it occurs unevenly, with the greatest mass loss observed on the side exposed to vapor flow. The data presented indicate the high corrosiveness of the vapours toward carbon steel,

attributed to the presence of aggressive components from coke oven gas entrained in the oil, such as hydrogen sulfide, ammonia, and hydrogen cyanide.

The content of mechanical impurities in the investigated operating oil ranges from 0.78 % to 0.95 %, whereas in the operating oil of a normally functioning plant, this value is significantly lower, ranging from 0.04 % to 0.08 %.

To ensure high resistance of materials to cavitation in real conditions of corrosion and erosion destruction of pipes during the operation of a tube furnace, steel grades such as AISI 321, AISI 309Ti, AISI 316 should be used. These materials will provide high resistance to cavitation in actual operating conditions. In addition, the results of the work will be useful in coking coal mixtures with oxidized coals [27 - 31].

CONCLUSIONS

Heating watered oil in a tube furnace causes severe corrosion damage to the metal, manifesting as hemispherical caverns. No intergranular corrosion is observed, but evidence of cavitation damage is noted.

Oil watering significantly increases the vapor phase fraction, particularly under conditions of decreasing flow pressure and rising temperature, which enhances cavitation and erosion of the tube bundle. The high polydispersity of water droplets (P_D = 4.8), their large size (up to 229 μm), and low specific interfacial surface area (0.16 μm^{-1}) heighten the oil's susceptibility to cavitation.

Hydraulic calculations reveal that, in a turbulent flow regime with a pressure of 1 bar, a water content of 20 %, and a temperature of 160°C, cavitation becomes inevitable. Cavitation accelerates corrosion, particularly in the presence of aggressive compounds such as ammonium chloride. Electrochemical analyses confirm the elevated corrosion rate of watered oil, while gravimetric measurements demonstrate the high corrosiveness of oil vapours toward carbon steel, driven by the release of aggressive coke oven gas components (e.g., H_2S, NH_3, HCN).

Authors' contributions

S.N. and M.B.: investigation, L.B.: conceptualization; D.M.: writing; O.B.: review; V.T.: data analysis.

REFERENCES

1. S.V. Nesterenko, L.P. Bannikov, Y.N. Skripiy, I.A. Klemin, Corrosive activity of coal-tar wash oils and life of equipment in benzene recovery, Coke Chem., 61, 2018, 141-146. https://doi.org/10.3103/S1068364X18040051.
2. V.V. Zelenskiy, S.V. Nesterenko, L.P. Bannikov, Corrosion resistance of nickel steel and nickel alloys in aggressive media, Coke Chem., 57, 2014, 167-176. https://doi.org/10.3103/S1068364X14040097.
3. S.V. Nesterenko, L.P. Bannikov, Y.N. Skripiy, Corrosion by the absorbing solution in vacuum–carbonate sulfur removal, Coke Chem., 58, 2015, 389-395. https://doi.org/10.3103/S1068364X15100075.
4. E.T. Kovalev, L.P. Bannikov, Experience in Ukrainian operating units of the coke oven gas desulfurization by alkanolamine aqueous solutions, Journ. Coal Chem., 1, 2018, 36-42. https://www.ukhin.org.ua/images/magazine/2018/1_2018/Journal1-2_2018-1.pdf, (in Ukrainian).
5. S.V. Nesterenko, V.M. Troshin, L.P. Bannikov, V.V. Karchakova, Improving the corrosion resistance of steel and alloys in coal-tar processing, Coke Chem., 59, 2016, 389-395. https://doi.org/ 10.3103/S1068364X16100070.
6. S.V. Nesterenko, V.V. Zelensky, M.V. Shapovalov, L.P. Bannikov, The main causes of pipelines corrosion of process gases of the coke plant, Journ. Coal Chem., 1, 2018, 56-62. https://www.ukhin.org.ua/images/magazine/2018/1_2018/Journal1-2_2018-1.pdf, (in Ukrainian).
7. L. Bannikov, D. Miroshnichenko, A. Bannikov, O. Borisenko, V. Tertychny, Dephenolization of coal tar heavy fractions: a reagent-free method for phenol recovery. J. Chem. Technol. Metall., 60, 3, 2025, 471-480. https://doi.org/10.59957/jctm.v60.i3.2025.13
8. A. Murad, U.H. Anwar, K. Tayyab, B. Abdulhakim, B. Haider, B.O. Eyitope, S. Aamer, Corrosion-related failures in heat exchangers, Corros. Rev., 39, 6, 2021, 519-546. https://doi.org/10.1515/corrrev-2020-0073.
9. F.V. Yusubov, Improving tube furnaces for delayed coking, Coke Chem., 66, 2023, 205-215. https://doi.org/10.3103/S1068364X23700734.
10. M.A. Dimastiar, A. Taufik, A.Z. Syahrial,

Failure analysis of tube radiant heater hot oil in refinery industry, Proceedings of the IIW 2018 - International Conference on Advanced Welding and Smart Fabrication Technologies, MATEC Web of Conferences, 269, 03013, 2019, 1-7. https://doi.org/10.1051/matecconf/201926903013.

11. B. Issa, V. Bazhin, T. Aleksandrova, Increasing the corrosion resistance of tubular furnace elements at temperature range 400-700°C in accelerated testing for real operational conditions, in: A. Author (Ed.), Advances in Raw Material Industries for Sustainable Development Goals, CRC Press, 2020, 174-185. https://doi.org/10.1201/9781003164395-23.
12. A. Ul-Hamid, H.M. Tawancy, Corrosion of industrial furnace tubes in a chlorine contaminated environment, Mater. High Temp., 25, 2, 2008, 89-99. https://doi.org/10.3184/096034008X335252.
13. L.N. Sari, The failure of furnace tube caused by deposit and sulfide corrosion in Migas industry, Mater. Komp. Konstruksi, 14, 1, 2014, 1-7. https://doi.org/10.29122/mkk.v14i1.1649.
14. M. Mohammadi, M.K. Khorrami, H. Vatanparast, A. Karimi, M. Sadrara, Classification and determination of sulfur content in crude oil samples by infrared spectrometry, Infrared Phys. Tech., 127, 2022, 104382. https://doi.org/10.1016/j.infrared.2022.104382.
15. Q. Shi, J. Wu, Review on sulfur compounds in petroleum and its products: state-of-the-art and perspectives, Energ. Fuel., 35, 18, 2021, 14445-14461. https://doi.org/10.1021/acs.energyfuels.1c02229.
16. F. Zhang, Determination of sulphur in coal tar by tube furnace combustion-infrared absorption method, Metall. Analysis, 31, 6, 2011, 48-50. https://www.researchgate.net/publication/293315608.
17. L.P. Bannikov, D.V. Miroshnichenko, A.L. Bannikov, Evaluation of the effect of resin forming components on the quality of wash oil for benzene recovery from coke oven gas, Pet. Coal, 65, 2023, 387-399. https://www.vurup.sk/wp-content/uploads/2023/05/PC-X_Miroshnichenko_74.pdf.
18. M.E. Machado, E.B. Caramão, C.A. Zini, Investigation of sulphur compounds in coal tar using monodimensional and comprehensive two-dimensional gas chromatography, J. Chromatogr. A, 1218, 21, 2011, 3200-3207. https://doi.org/10.1016/j.chroma.2010.11.077.
19. R.B. Rebak, Sulfidic corrosion in refineries – a review, Corros. Rev., 29, 2011, 123-133. https://doi.org/10.1515/corrrev.2011.021.
20. D. Adnyana, Cavitation-erosion study in elbow tubes of a low-pressure evaporator outlet header, Metalurgi, 35, 1, 2020, 33-42. https://doi.org10.14203/metalurgi.v35i1.561.
21. ASTM International, ASTM G4-95: Standard Guide for Conducting Corrosion Coupon Tests in Field Applications, ASTM Int., 1995, Available: www.astm.org/g0004-95.html.
22. N. Bilousova, Estimation of corrosion rate and Tafel coefficients by polarization methods. Eur. Sci., 1, 2023, 70-83. https://doi.org/10.30890/2709-2313.2023-21-01-024.
23. ASTM International, ASTM E768-99(2018): Standard Guide for Preparing and Evaluating Specimens for Automatic Inclusion Assessment of Steel, ASTM Int., 2018. Online. Available: https://www.astm.org/e0768-99r18.html.
24. A. Šarc, T. Stepišnik-Perdih, M. Petkovšek, M. Dular, The issue of cavitation number value in studies of water treatment by hydrodynamic cavitation, Ultrason. Sonochem., 34, 2017, 51-59. https://doi.org/10.1016/j.ultsonch.2016.05.020.
25. S.P. Siva, Y.K. Ho, K.W. Kow, C.H. Chan, S.Y. Tang, Prediction of droplet sizes for oil-in-water emulsion systems assisted by ultrasound cavitation: transient scaling law based on dynamic breakup potential, Ultrason. Sonochem., 55, 2018, 348-358. https://doi.org/10.1016/j.ultsonch.2018.12.040.
26. Z. Zhang, G. Wang, Y. Nie, J. Ji, Hydrodynamic cavitation as an efficient method for the formation of sub-100 nm O/W emulsions with high stability, Chin. J. Chem. Eng., 24, 10, 2016, 1477-1480. https://doi.org/10.1016/j.cjche.2016.04.011
27. D.V. Miroshnichenko, Yu.S. Kaftan, N.A. Desna, A.V. Sytnik, Oxidation of bituminous coal. 1. Expansion pressure. Coke Chem., 58, 10, 2015, 376-381. https://doi.org/10.3103/S1068364X15100051
28. D.V. Miroshnichenko, I.D. Drozdnik, Yu.S. Kaftan, N.A. Desna, Oxidation of pokrovskoe coal in laboratory and natural conditions. 1. Kinetics of oxidation and technological properties. Coke Chem., 58, 3, 2015, 79-87. https://doi.org/10.3103/S1068364X15030059
29. D.V. Miroshnichenko, N.A. Desna, Yu.S. Kaftan,

Oxidation of coal in industrial conditions. 2. Modification of the plastic and viscous properties on oxidation. Coke Chem., 57, 10, 2014, 375-380. https://doi.org/10.3103/S1068364X14100056
30. N.A. Desna, D.V. Miroshnichenko, Oxidized coal in coking: A review, Coke Chem., 54, 5, 2011, 139-146. https://doi.org/10.3103/S1068364X11050036
31. D.V. Miroshnichenko, N.A. Desna, Yu.S. Kaftan, Oxidation of coal in industrial conditions. 4. Coal temperature in heap storage. Coke Chem., 58, 2, 2015, 43-48. https://doi.org/10.3103/S1068364X15020027